CHEMSUSCHEM
FULL PAPERS

ChemPubSoc Europe

DOI: 10.1002/cssc.201402100

A Continuous Flow Strategy for the Coupled Transfer Hydrogenation and Etherification of 5-(Hydroxymethyl)furfural using Lewis Acid Zeolites

Jennifer D. Lewis,[a] Stijn Van de Vyver,[a] Anthony J. Crisci,[a] William R. Gunther,[a] Vladimir K. Michaelis,[b] Robert G. Griffin,[b] and Yuriy Román-Leshkov*[a]

Hf-, Zr- and Sn-Beta zeolites effectively catalyze the coupled transfer hydrogenation and etherification of 5-(hydroxymethyl)-furfural with primary and secondary alcohols into 2,5-bis(alkoxymethyl)furans, thus making it possible to generate renewable fuel additives without the use of external hydrogen sources or precious metals. Continuous flow experiments reveal nonuniform changes in the relative deactivation rates of the transfer hydrogenation and etherification reactions, which impact the observed product distribution over time. We found that the catalysts undergo a drastic deactivation for the etherification step while maintaining catalytic activity for the transfer hydrogenation step. ^{119}Sn and ^{29}Si magic angle spinning (MAS) NMR studies show that this deactivation can be attributed to changes in the local environment of the metal sites. Additional insights were gained by studying effects of various alcohols and water concentration on the catalytic reactivity.

Introduction

The production of liquid fuels and additives from biomass-derived 5-(hydroxymethyl)furfural (HMF) is of significant interest.[1] Examples of HMF-derived fuels include C_9–C_{15} alkanes,[2] 2,5-dimethylfuran,[3] ethyl levulinate,[4] 5-(alkoxymethyl)furfurals,[4a,5] and 2,5-bis(alkoxymethyl)furans.[5e] Ethers of HMF and HMF derivatives are particularly attractive because of their high energy densities and advantageous fuel blending properties.[6] For instance, 2,5-bis(ethoxymethyl)furan (BEMF) has been assessed as a diesel additive in a six-cylinder heavy duty engine. The European Stationary Cycle test revealed no significant difference in engine operation for all tested blending ratios.[6] Considering the potential of HMF ethers as drop-in fuel replacements, the development of a continuous and scalable production process is highly desirable.

To date, most HMF etherification reactions involve functionalizing the hydroxyl group of HMF to produce a monoether derivative.[5c,d,g–j] Although catalytic synthesis of the diether is more desirable,[7] it is more challenging because it requires hydrogenating the carbonyl group into an alcohol prior to etherification. Balakrishnan et al. reported that a combination of Pt/Al_2O_3 and Amberlyst-15 can catalyze the conversion of HMF into 2,5-bis(alkoxymethyl)furan in the presence of molecular hydrogen and an alcoholic solvent.[5e] In parallel, Gruter considered a two-step process in which Pt/C is used to catalyze the hydrogenation of HMF into the intermediate 2,5-bis(hydroxymethyl)furan (BHMF).[8] The Meerwein–Ponndorf–Verley (MPV) reaction presents an attractive alternative approach to reduce carbonyl groups. Rather than using molecular hydrogen, this reaction uses an alcohol as a transfer hydrogenation (TH) agent.[9] Although several catalysts are active for TH reactions,[10] zeolites containing tetrahedrally coordinated d^0 or d^{10} metal centers (e.g., Sn or Zr) with Lewis acid character have emerged as highly active and selective inter- and intramolecular TH catalysts.[11] For instance, our group recently demonstrated the use of Zr-Beta zeolite for the production of γ-valerolactone from furfural through TH chemistry.[12]

Corma et al.[9b–d] and Jae et al.[9a] have investigated Sn- and Zr-Beta zeolites for TH/etherification cascade reactions.[13] Although promising results could be obtained in conventional batch systems, little is known about the long-term stability and modes of deactivation for these catalysts. In this contribution, we investigate the use of solid Lewis acids for the continuous production of 2,5-bis(alkoxymethyl)furans by coupled TH and etherification reactions using primary and secondary alcohols. Reaction and deactivation kinetics as well as long-term stability for Lewis acid zeolites are investigated under continuous operating conditions using plug-flow reactors. Detailed characterization studies are performed to reveal and correlate structural changes in the zeolites with observed changes in product distribution.

[a] J. D. Lewis,[+] Dr. S. Van de Vyver,[+] Dr. A. J. Crisci, W. R. Gunther, Prof. Y. Román-Leshkov
Department of Chemical Engineering
Massachusetts Institute of Technology
77 Massachusetts Avenue, Cambridge, MA 02139 (USA)
E-mail: yroman@mit.edu
Homepage: http://www.romangroup.mit.edu

[b] Dr. V. K. Michaelis, Prof. R. G. Griffin
Department of Chemistry and Francis Bitter Magnet Laboratory
Massachusetts Institute of Technology
77 Massachusetts Avenue, Cambridge, MA 02139 (USA)

[+] These authors contributed equally to this work.

Supporting Information for this article is available on the WWW under http://dx.doi.org/10.1002/cssc.201402100.

Results and Discussion

Catalyst screening in batch mode

The coupled TH/etherification strategy was investigated with a series of zeolites containing various Lewis acid centers. We report the synthesis of a new zeolite, Hf-Beta, in addition to conventionally used Lewis acid zeolites such as Sn- and Zr-Beta. The rationale for studying these different metal centers is that the extent of intermolecular conversion between carbonyl and hydroxyl functionalities during MPV reactions is dictated by the relative thermodynamic stability between products and reactants while reaction kinetics are altered by the ability of the Lewis acid center to appropriately coordinate and polarize the C–O bonds.[14]

Preliminary studies of the catalytic performance of the solid Lewis acids were conducted under batch conditions (Table 1). The proposed network for the coupled TH and etherification of HMF with ethanol is shown in Scheme 1. Pathways a and b proceed through a sequence of one TH and two etherification reactions. In pathway c, acetalization of HMF produces 5-(hydroxymethyl)furfural diethyl acetal (HMFDEA; see Figure S1 in the Supporting Information for the ^{1}H NMR spectrum), which reacts with ethanol to give the intermediate 5-(ethoxymethyl)-furfural diethyl acetal (EMFDEA). The product distribution obtained with ethanol is consistent with the reaction network proposed by Jae et al. for the etherification of HMF with isopropanol.[9a]

High BEMF yields are associated with Hf-, Zr-, and Sn-Beta having the highest catalytic activity for the TH step of all catalysts tested (Table 1, entries 1–3). Ta- and Al-Beta are less effective TH catalysts but do promote etherification reactions as evidenced by the higher proportion of 5-(ethoxymethyl)furfural (EMF) and EMFDEA products (Table 1, entries 5 and 9). Ti- and Nb-Beta were ineffective at catalyzing either the TH or the etherification steps, thereby resulting in overall low HMF conversion levels. Computational studies have shown that Sn- and Zr-containing zeolites feature the lowest energetic barriers for the TH reaction between alcohols and ketones when the reaction occurs on an open site (i.e., a tetrahedral framework metal site with one hydrolyzed M–O–Si bond).[9b] Enhanced TH reactivity on open sites is ascribed to two factors: 1) the favorable activation of the alcohol through a base-catalyzed deprotonation promoted by silanol groups adjacent to the open site; and 2) a favorable interaction of the ketone with the metal center such that the ketone can displace one of the two alcohol solvent molecules adsorbed on the active site to generate the required six-membered transition state for the rate-limiting hydride shift step. The overall barriers for the reaction depend on many factors, including the Lewis acid character of the metal center (which dictates the barriers for the transition state and the adsorption enthalpies of the reagents) and the zeolite topology (which dictates the number and basicity of the silanol groups adjacent to the metal center in the open site). Taken together, our data are in agreement with the computational reports on the relative rates for TH reactions, showing that hard Lewis acid centers, such as Sn and Zr, optimally stabilize the rate-limiting hydride shift transition state whereas weaker Lewis acid centers, such as Ti and Ta, do not readily cata-

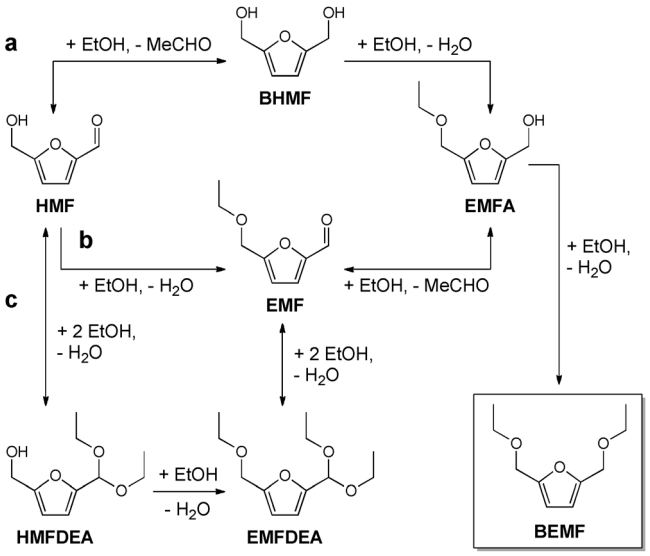

Scheme 1. Proposed reaction network for the coupled TH and etherification of HMF with ethanol. EtOH = ethanol, MeCHO = acetaldehyde. For other abbreviations, see the legend of Table 1.

Table 1. Conversion and product yields in the coupled TH and etherification of HMF with ethanol.[a]

Entry	Catalyst	Si/metal ratio[b]	*t* [h]	Conv. [%]	Yield[c] [%] BEMF	EMFA	BHMF	EMF	HMFDEA	EMFDEA	EL
1	Hf-Beta	107	24	87	67	6	1	1	5	<1	0
2	Zr-Beta	129	24	81	54	6	1	1	10	1	0
3	Sn-Beta	119	24	69	41	1	<1	21	<1	0	0
4	Ti-Beta	126	24	16	0	0	1	0	10	0	0
5	Ta-Beta	(100)	24	85	2	0	0	56	3	16	4
6	Nb-Beta	(100)	24	31	3	2	1	3	17	1	0
7	Sn-MCM-41	100	24	5	0	0	2	0	3	0	0
8	Zr-MCM-41	100	24	41	8	8	1	4	11	1	0
9	Al-Beta	13	3	94	7	0	0	41	4	35	2
10	Amberlyst-15[d]	–	3	92	0	0	0	32	6	33	10
11	HfO_2/Si-Beta	(106)	24	75	2	1	0	21	19	20	6
12	Si-Beta[e]	–	24	3	0	0	0	0	<1	0	0
13	none	–	24	1	0	0	0	0	0	0	0

[a] Reaction conditions: 1 wt% HMF in ethanol, (mol HMF)/(mol metal) = 100:3, 0.25 wt% 1,3,5-tri-*tert*-butylbenzene, 393 K. [b] Values in parentheses refer to the nominal metal loading in the synthesis gel. [c] BEMF = 2,5-bis(ethoxymethyl)furan; EMFA = 5-(ethoxymethyl)furfuryl alcohol; BHMF = 2,5-bis(hydroxymethyl)furan; EMF = 5-(ethoxymethyl)furfural; HMFDEA = 5-(hydroxymethyl)furfural diethyl acetal; EMFDEA = 5-(ethoxymethyl)furfural diethyl acetal; EL = ethyl levulinate. [d] Reaction performed with a ratio of 100:3 (mol HMF)/(mol acid sites). [e] Catalyst loading (wt%) matched to that for Hf-Beta.

lyze TH reactions, particularly when using a primary alcohol as hydrogen donor.

The decreased conversion and low BEMF selectivity for Sn- and Zr-MCM-41 (Table 1, entries 7 and 8) indicate that the pore hydrophobicity of the crystalline framework of zeolite Beta is crucial to maintain its activity in the presence of water (i.e., a by-product in the etherification and acetalization reactions). The observed difference in reactivity can also be attributed to differences in bond distance and geometry of the metal in the zeolite Beta and MCM-41 materials. Extra-framework HfO_2 nanoparticles impregnated on Si-Beta (HfO_2/Si-Beta) failed to generate BEMF in any appreciable yield (Table 1, entry 11), indicating that the Hf atoms need to be isolated within the zeolite framework to be catalytically active. We also confirmed that the reaction is not catalyzed by purely siliceous zeolite Beta (Table 1, entry 12) and does not occur in the absence of catalyst (Table 1, entry 13). Brønsted acid catalysts Al-Beta and Amberlyst-15 (hydrogen form) were highly active for etherification and acetalization reactions (Table 1, entries 9 and 10); however, they were not active in the TH step. The high conversion of 94% observed after 3 h reaction with Al-Beta reflects the strong Brønsted acidity of the normal framework aluminum sites.[15] Besides the products and intermediates depicted in Scheme 1, significant amounts (up to 10%) of ethyl levulinate (EL) were formed through Brønsted acid-catalyzed alcoholysis of HMF.[5e]

Insights into the reaction network

A typical time course for the conversion of HMF using Hf-Beta is provided in Figure 1. Almost 56% HMF is consumed within the first hour, yielding 41% of the HMFDEA intermediate. Between 1 and 24 h, we observe a decrease in the selectivity to HMFDEA from 73% to 6% and a corresponding increase in selectivity to BEMF from 5% to 77%. These data suggest that the conversion of HMFDEA proceeds through acid-catalyzed hydrolysis of the acetal moiety in the reverse direction of pathway c shown in Scheme 1 followed by a TH and etherification with ethanol to yield BEMF. We have also considered a direct conversion of the acetal into BEMF. Previous work by Balakrishnan et al.[5e] showed that Pt/Al_2O_3 catalysts can catalyze the hydrogenolysis of HMFDEA and EMFDEA into EMF and BEMF, respectively. Evidently, when the reaction is catalyzed by Lewis acids in the absence of molecular hydrogen, hydrogenolysis is less likely to occur. This was experimentally confirmed using the model substrate 2-furaldehyde diethyl acetal in a reaction with ethanol and Hf-Beta. No detectable levels of ether product were formed after short reaction times, whereas significant quantities of the aldehyde and alcohol intermediates could be observed (Supporting Information, Figure S2). The ether compound is a secondary product that appears at a later reaction stage, supporting our hypothesis that the acetal must first be hydrolyzed and reduced to the alcohol before forming an ether. Acetalization, a common carbonyl protection method,[16] competes with the MPV reduction and retards the direct production of BEMF. Interestingly, a similar etherification pathway has been previously reported as a side reaction in the Zr-Beta-catalyzed MPV reduction of cinnamyl alcohol in the presence of 2-propanol.[17]

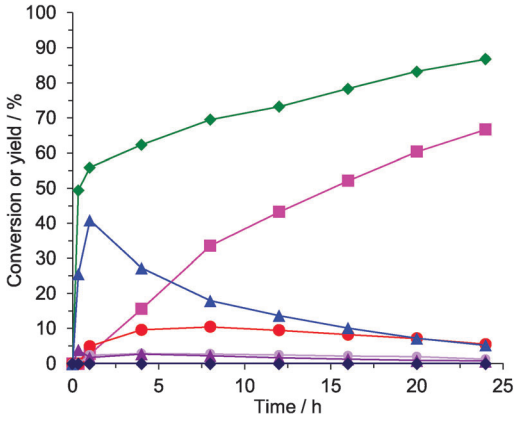

Figure 1. Evolution of the HMF conversion (◆) and yields of BEMF (■), EMFA (●), BHMF (●), EMF (▲), HMFDEA (▲), and EMFDEA (◆) as a function of time in the coupled TH and etherification of HMF with ethanol using Hf-Beta. Reaction conditions: see Table 1.

Flow-reactor studies of the coupled TH and etherification of HMF with ethanol

To study the long-term stability of the Lewis acid zeolites and infer their deactivation mechanism, reactions were performed in continuous flow mode by using a fixed bed plug flow reactor (see the Experimental Section for full details). So far, this type of Lewis acid-catalyzed reaction has only been studied in batch reactors. For example, catalyst stability studies by Jae et al. have been performed by recycling and reusing the Sn-Beta catalyst after a single batch reaction of HMF in a 2-propanol solution.[9a] Their results indicate that the deactivation of Sn-Beta is due to the deposition of heavy by-products and calcination of the spent catalysts at 823 K resulted in a complete recovery of the catalytic activity and selectivity to the desired 2,5-bis[(1-methylethoxy)methyl]furan. Our goal was to provide information on the long-term behavior of the catalyst and the detrimental effects of water on the Lewis acid reactivity.

Figure 2 shows a plot of the catalytic activity of Hf-Beta and Sn-Beta for HMF to BEMF conversion as a function of time on stream (TOS). Note that the weight hourly space velocity (WHSV, defined as the mass of the feed solution per mass of catalyst per hour) was adjusted so that both catalysts achieved similar initial conversions. Figure 2a reveals that over the course of the reaction Hf-Beta experienced different stages of deactivation. The initial transient regime was characterized by a decrease in HMF conversion with a simultaneous decrease in BEMF yield. After 2 h, an apparent steady state was established with yields of 22% and 24% for production of BEMF and HMFDEA, respectively. However, for TOS beyond 15 h, HMF conversion decreased to values under 30% accompanied by a shift in product selectivity to predominantly BHMF. Practically no etherification products could be detected after 20 h on stream. At this point, it is important to mention that the turnover number (TON) based on the total Hf content was 45 at

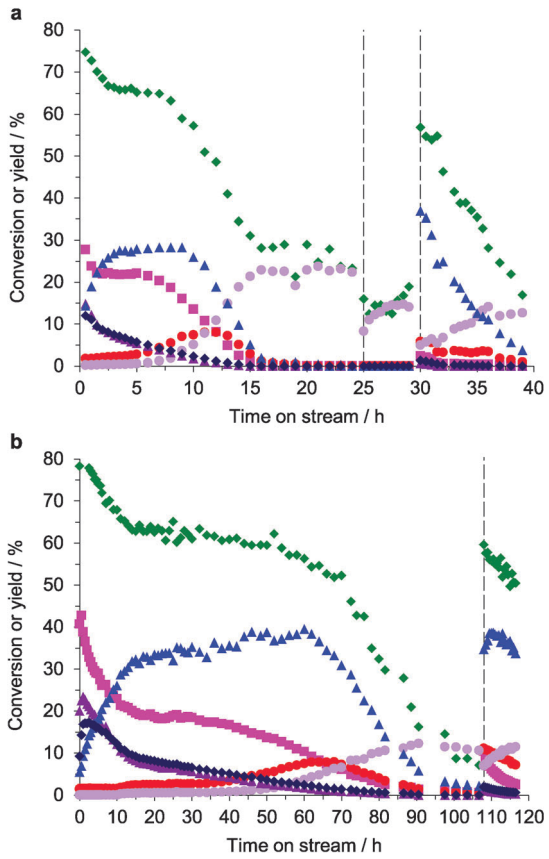

Figure 2. HMF conversion (◆) and yields of BEMF (■), EMFA (●), BHMF (●), EMF (▲), HMFDEA (▲), and EMFDEA (◆) as a function of TOS for flow reactions with a) Hf-Beta and b) Sn-Beta. Reaction conditions: 1 wt% HMF in ethanol, 0.25 wt% 1,3,5-tri-*tert*-butylbenzene, 393 K, 791 kPa. The operating conditions of the flow reactor were: For Hf-Beta, 613 mg catalyst (Si/Hf ratio of 93), WHSV of 18.9 h^{-1}, flow rate of 0.24 mL min^{-1}; and for Sn-Beta, 620 mg catalyst (Si/Sn ratio of 90), WHSV of 10.7 h^{-1}, flow rate of 0.14 mL min^{-1}. Regeneration of Hf-Beta was performed by flushing the catalyst bed with ethanol and by in situ calcination in air at 823 K for 5 h (indicated by the dashed lines). Regeneration of Sn-Beta was performed by calcination.

the end of the steady-state regime and 105 after 24 h. We note, however, that the real TON would probably be higher, as only some of the Hf sites are active for the MPV reduction.[11f] Indeed, it has been theorized that the partially hydrolyzed metal centers are the active sites in the MPV reaction and only a fraction of the metal atoms are in that configuration.

Regeneration of the deactivated Hf-Beta catalyst was performed in two ways: (i) by flushing the catalyst bed with ethanol, followed by drying with air at 423 K; and (ii) by in situ calcination in air at 823 K for 5 h. Figure 2a shows that after the first regeneration step Hf-Beta is still inactive for etherification, suggesting that the deactivation is not likely to occur through the adsorption of HMF and its derivatives on the Hf sites. Indeed, one would expect that such compounds would exchange with ethanol upon prolonged flushing. After calcination, there is a significant enhancement in catalytic activity, although the selectivity to BEMF remained <5%. The calcined Hf-Beta catalyst shows a deactivation profile similar to that of the original sample after 10 h on stream. Specifically, the dominant product is HMFDEA with selectivities up to 65% and the pseudo-first-order decay rate is about 0.16 h^{-1} (Supporting Information, Figure S3). Based on the partially recovered activity after calcination, we anticipated that at least part of the reversible deactivation of the catalyst could occur through the deposition of organic compounds (vide infra).

We next evaluated the deactivation kinetics of Zr- and Sn-Beta. Zr-Beta showed a deactivation profile similar to that observed for Hf-Beta; however, a significantly lower catalytic activity was achieved after calcination (Supporting Information, Figure S5). In the case of Sn-Beta, a lower WHSV of 10.7 h^{-1} was required to achieve a similar degree of HMF conversion (Figure 2b). Its lower catalytic activity compared to Hf- or Zr-Beta is also reflected in a seemingly less drastic deactivation profile. At an equivalent TON of 85, Sn-Beta had a product distribution of 18% BEMF, 6% EMF, and <1% BHMF at a TOS of 22 h whereas Hf-Beta generated yields of <1%, <1%, and 23%, respectively, at a TOS of 16 h. The Sn-Beta catalyst featured a comparable product distribution to Hf-Beta but with a higher selectivity towards BEMF (31% vs. 4%) after regeneration by calcination.

Overall, our results indicate different deactivation kinetics for the TH and etherification reactions. Additional control experiments were performed under similar reaction conditions as in Figure 2 but using BHMF instead of HMF as co-reactant (Supporting Information, Figure S6). We attempted the continuous etherification of BHMF with ethanol using Hf-Beta; however, this experiment resulted in a very fast deactivation of the catalyst with a decrease in conversion from 90% to less than 10% over a period of roughly 2 h. Jae et al. reported similar observations upon reusing Sn-Beta after batch reactions with 1.2 wt% BHMF in 2-propanol and hypothesized that the faster deactivation of the catalyst in the presence of BHMF could be attributed to the formation of heavy by-products from the self-etherification of the dialcohol at 453 K (100:1 molar ratio of BHMF to Sn).[9a] However, as observed in Figure 2, although Hf- and Sn-Beta deactivate with respect to the etherification step, both catalysts remain active for the TH step under our reaction conditions. For instance, Hf-Beta converted HMF into BHMF with high selectivity under steady-state conditions in the range of 16–24 h on stream in spite of producing BEMF in yields <1%. Because the presence of heavy by-products occluded in the pores could not fully account for the deactivation of only the etherification reaction in our system, we proceeded with detailed catalyst characterization studies.

Post-reaction catalyst characterization

The catalysts were characterized by means of powder X-ray diffraction (PXRD); ultraviolet/visible (UV/Vis) spectroscopy; inductively coupled plasma atomic emission spectrometry (ICP-AES); thermogravimetric analysis (TGA); ^{13}C, ^{119}Sn, and ^{29}Si magic-angle spinning nuclear magnetic resonance (MAS NMR); Fourier transform infrared (FTIR) spectroscopy; and N_2 physisorption measurements. The PXRD patterns of Sn-, Zr-, and Hf-Beta show that the long-range topological order of the Beta zeolite is well preserved after the flow reactions (Supporting Informa-

tion, Figure S7). Moreover, the UV/Vis spectra of the spent Sn-, Zr-, and Hf-Beta catalysts do not show significant differences compared to the spectra of the original samples (Supporting Information, Figure S8). For example, in the UV/Vis spectra of Sn-Beta, absorption bands associated with tetrahedrally coordinated Sn are observed before and after reaction. ICP-AES analyses show only minimal differences in Si/M ratios for the zeolites before and after reaction (Table 2). Collectively, these results suggest that catalyst deactivation cannot be attributed to metal leaching or significant formation of metal oxide nanoparticles.

Table 2. Summary of results obtained by TGA and ICP-AES analysis.

Sample	Adsorbed species[a] [wt%]	Si/metal ratio[b] before reaction	after reaction
Hf-Beta	5.3	93±1	102±2
Zr-Beta	3.2	120±2	117±1
Sn-Beta	2.7	90±3	92±3

[a] Determined by TGA analysis (see the Supporting Information, Figure S9). [b] Metal loading determined by ICP-AES analysis and based on the average of three independent measurements.

One of the most common problems associated with acid-catalyzed transformations of HMF is the formation of humins or humin-like components.[18] Spent Hf-, Zr-, and Sn-Beta samples were washed with ethanol and dried at 423 K prior to removal from the flow reactor. We investigated the potential adsorption of carbonaceous components on the zeolites using TGA and $^{13}C\{^1H\}$ cross polarization (CP)/MAS NMR. The extracted catalysts were only slightly off-white in appearance, which suggests that humins were not produced in significant concentrations. TGA was performed by heating the samples from room temperature to 1073 K under nitrogen-diluted air while monitoring the weight losses (Table 2 and Figure S9 in the Supporting Information). The results reveal a marginal initial weight loss of approximately 1% after heating to 423 K due to the loss of physisorbed water. TGA thermograms further indicate weight losses of 2–5 wt% over a temperature range of 423–823 K. For example, pristine Sn-Beta showed a weight loss of 0.9% in this temperature range, suggesting the observed weight loss is related to water generated by the condensation of silanols. In the presence of ethanol, silanols readily exchange to generate $\equiv SiOCH_2CH_3$ sites. Assuming complete exchange, we would expect the spent catalyst to show a weight loss of 2.3%; however, we observed a 1.7% difference. By $^{13}C\{^1H\}$ CP MAS NMR, we observed resonances at $\delta = 61$ and 19 ppm on spent Sn-Beta (Figure 3), which are attributable to such $\equiv SiOCH_2CH_3$ sites. Similar to Tucker et al.,[19] humins or humin-like deposits were not detected within a porous catalyst operated in flow. Given that we achieved carbon balances with an average of more than 98% in flow, it is likely that such by-products were not produced and were not responsible for the deactivation of the zeolites.

To investigate the local environment of the metal sites in the zeolites, we prepared a Sn-Beta sample with an enriched

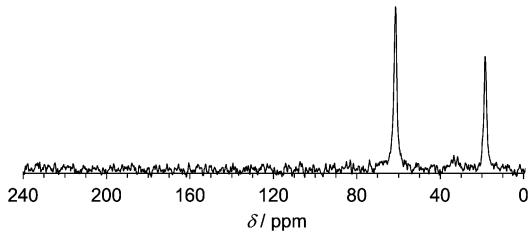

Figure 3. $^{13}C\{^1H\}$ CP/MAS NMR spectrum of the Sn-Beta catalyst recovered after the last cycle in Figure 2b. The sample was flushed with ethanol prior to analysis.

^{119}Sn precursor (80% enrichment) and tested it in the flow reactor under the same conditions as in Figure 2b. ^{119}Sn-Beta possessed a reactivity profile similar to unenriched Sn-Beta. The reaction was operated continuously for 96 h until the BEMF yield reached less than 1%. Figure 4 shows the dehydrated ^{119}Sn MAS and CP/MAS NMR spectra of the Sn-Beta catalyst before and after reaction. Note that both samples were calcined prior to analysis. The ^{119}Sn NMR spectrum for the pristine catalyst exhibits a resonance at $\delta = -444$ ppm that corresponds to framework Sn atoms, in agreement with previously reported assignments.[11d,20] Notably, the spent catalyst exhibits two additional resonances located at $\delta = -436$ and -421 ppm. All of these resonances correspond to four-coordinated Sn,[20a] within a pseudotetrahedral environment. In the ^{119}Sn CP/MAS NMR spectra, we observe an increase in the intensities for the resonances at $\delta = -436$ and -421 ppm, indicating the presence of protons near the Sn centers. The increase in intensity for the -421 ppm signal is significantly higher than that observed for the -436 ppm resonance.

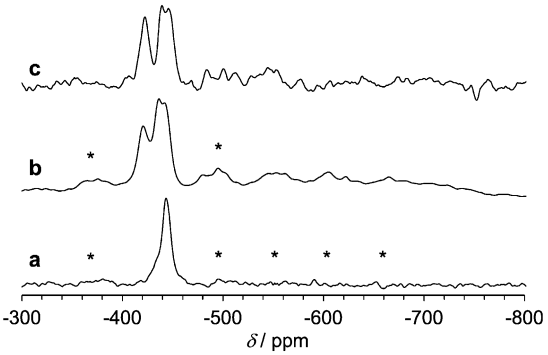

Figure 4. ^{119}Sn MAS NMR spectra of ^{119}Sn-Beta: a) Pristine catalyst; b) spent catalyst after 96 h TOS under identical conditions as in Figure 2b; c) same sample as in (b) but measured with cross polarization ($^{119}Sn\{^1H\}$, $\tau_c = 2$ ms). The samples were calcined at 823 K prior to analysis. Asterisks (*) mark the prominent spinning sidebands.

The shift located at $\delta = -421$ ppm has previously been attributed to monohydrolyzed framework Sn sites,[20a] but for the present data it cannot be excluded that these signals represent a dihydrolyzed Sn site at $\delta = -421$ ppm and a monohydrolyzed Sn site at -436 ppm (Scheme 2). Alternatively, the signal at -421 ppm could represent the monohydrolyzed site and the -436 ppm resonance may be related to the distortion of

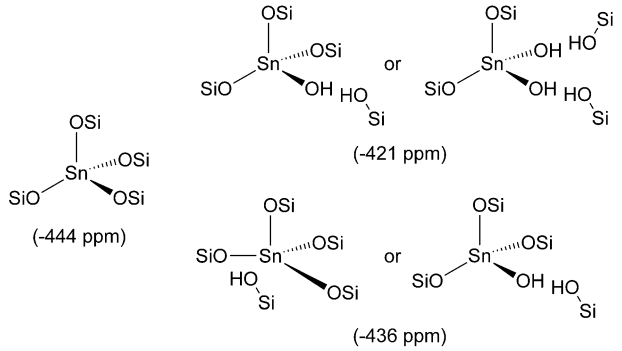

Scheme 2. Representation of the proposed Sn sites in Sn-Beta. The chemical shifts corresponding to the ^{119}Sn NMR spectra in Figure 4 are given in parentheses (tentative assignment).

framework Sn sites due to framework rearrangement. The signal enhancement observed in the CP/MAS NMR experiment would then be expected if silanols were generated near these framework Sn sites due to such a rearrangement. The occurrence of site distortion is supported by the considerable increase in chemical shift anisotropy signified by the increase in prominent spinning sidebands (marked with an * in Figure 4). Altogether, it is clear that homogeneity of the framework Sn sites is lost as a result of the reaction.

^{29}Si MAS NMR spectroscopy was performed to determine whether degradation of the framework was limited to the Sn sites or present throughout the zeolite (Figure 5). The overall

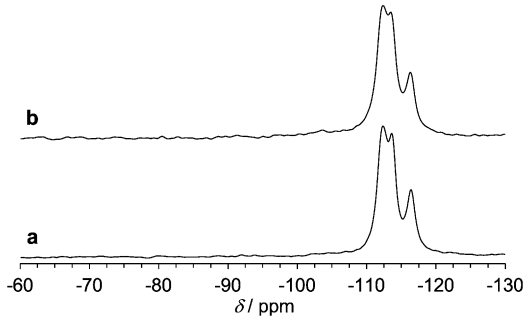

Figure 5. ^{29}Si MAS NMR spectra of ^{119}Sn-Beta: a) Pristine catalyst; b) spent catalyst after 96 h TOS under identical conditions as in Figure 2b. The samples were calcined at 823 K prior to analysis.

Si framework is identical for the treated and untreated Sn-Beta, indicating that the long- (PXRD) and short-range (MAS NMR spectroscopy) crystalline topology is maintained. We note that silanols could have been generated during the reaction, but these are not observed in the ^{29}Si MAS NMR spectrum because neighboring hydroxyl groups were condensed during the calcination step. This hypothesis can also be applied to the local environment of the Sn center, which might become even more disordered during the reaction.

N_2 adsorption/desorption experiments were performed on the pristine and spent Sn-Beta catalyst (Supporting Information, Figure S10). The spent catalyst shows less hysteresis of the desorption branch and has a lower micropore volume (0.15 $cm^3 g^{-1}$) than that of the pristine sample (0.19 $cm^3 g^{-1}$). This reduction in porosity probably occurs throughout the reaction. As approximately 75% of the initial conversion is regenerated by calcination, the loss of micropore volume does not significantly contribute to the catalyst deactivation on the experimental time scale.

The effect of the structural changes on the Lewis acidity of the zeolite was investigated by FTIR spectroscopy. FTIR analysis of adsorbed deuterated acetonitrile (CD_3CN) has been used to characterize the acidity of framework species in Sn-Beta.[21] Herein, CD_3CN was adsorbed onto self-supporting wafers of calcined Sn-Beta samples before and after reaction to track potential changes in Lewis acidity. In agreement with literature reports,[21a] ν(C≡N) stretching vibrations for adsorbed CD_3CN on fresh Sn-Beta are observed at 2309 and 2274 cm^{-1}, representing the adsorbate coordinated to framework Sn atoms and silanols, respectively (Figure 6). After the reaction, these ν(C≡N) vibrations are centered at 2304 and 2279 cm^{-1}. In comparison

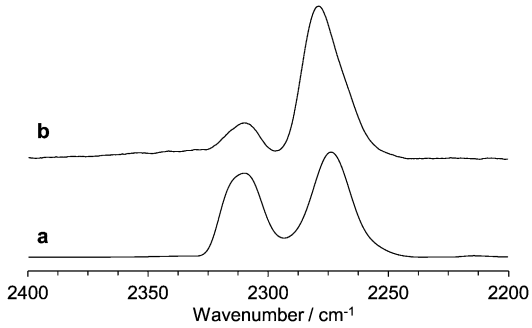

Figure 6. FTIR spectra of Sn-Beta recorded under vacuum after exposure to CD_3CN vapor at RT: a) Pristine catalyst; b) catalyst recovered after the last cycle in Figure 2b. The samples were calcined at 823 K prior to analysis.

to the fresh catalyst, the relative amount of Lewis acid sites to Brønsted acidic hydroxyl groups for the spent catalyst is significantly lower, whereas the slight red-shift from 2309 to 2304 cm^{-1} suggests that the remaining Lewis acid sites in the spent catalyst generate a weaker interaction with the adsorbate compared to the pristine material.[22] Although these sites are weaker, they are still largely active (see the in situ calcined catalyst in Figure 2b). Specifically, the calcined catalyst showed similar activity and BEMF selectivity as the pristine Sn-Beta after approximately 60 h TOS.

Insights into the etherification mechanism and the acidic nature of the active sites

The literature available on Lewis acid-catalyzed etherification is scarce,[9] and the reaction mechanism is poorly understood. Conversely, the use of homogeneous and heterogeneous Brønsted acids as etherification catalysts has been thoroughly investigated.[5c,d,23] The reaction pathway for the Brønsted acid-catalyzed coupling of two alcohols proceeds via protonation of

the hydroxyl group and intermolecular etherification through S_N1 or S_N2 reactions.[9c] Based on the present reaction and characterization results the involvement of Brønsted acids in the catalytic etherification of HMF cannot conclusively be excluded. We hypothesize that the acid–base characteristics of the hydroxyl groups on or near the metal centers may play a role in the etherification steps in Scheme 1.

According to our post-reaction catalyst characterization, the distortion or cleavage of one or more bridging oxygen atoms clearly occurs at the Sn centers and it is expected that these changes will also occur for Hf-Beta. Yet it remains unclear how or when these physical changes occur during operation. Further investigation is also needed to determine the influence of the hydroxyl sites and bridging oxygen atoms at the active site on reaction rates. Reports have stated that the hydroxyl group on Sn-Beta is basic[21d,e] whereas with Zr-Beta, and most likely Hf-Beta, the distribution of electron density gives an acidic character to the bridging oxygen atoms.[17,24] Zhu et al. characterized these Brønsted acid sites by performing pyridine IR spectroscopy and demonstrated that these sites can catalyze the formation of ethers through the dehydration of hemiacetals (i.e., similar to the pathway discussed above).[17] In the case of Sn-Beta, it is interesting to note that studies by de Clippel et al. revealed an improved catalytic activity of Sn centers in the presence of weak Brønsted acid sites.[25] It can be further argued that if hydroxyl groups play a role in the etherification reaction, the gradual deactivation of this pathway may be a result of the exchange between ethanol and the proton of the hydroxyl group. Indeed, our $^{13}C\{^1H\}$ CP/MAS NMR results were indicative of the formation of $\equiv SiOCH_2CH_3$ sites (Figure 3). This would explain why the original etherification activity could be partially restored by calcination of the zeolites but not by flushing with ethanol. To obtain a better understanding of this deactivation mechanism, follow-up studies will be critical to identify, characterize, and quantify the hydroxyl sites and bridging oxygen atoms. Another pertinent question is whether these catalytic sites exhibit different sensitivities to the presence of water generated during reaction. For example, it has been shown that neighboring or geminal silanols tend to adsorb more water than isolated hydroxyl groups.[26] As a result, the residence time of in situ formed water may increase as more hydroxyl groups are generated. This may hasten structural rearrangement (observed as a loss of surface area and pore volume) and/or inhibit the reactions.

Effects of water and molecular structure of the alcohol

The shift in selectivity from BEMF to BHMF observed in the flow reactions and the post-reaction catalyst characterization results prompted us to investigate the influence of water on the catalyst performance. Given that water has been shown to have a strong impact on the reactivity of some Lewis acid zeolites,[11e] the selectivity shift we observe could be related to in situ generation and accumulation of water near the active sites over time. Table 3 depicts the results of batch experiments of HMF TH and etherification in ethanol using Hf- and Sn-Beta in the presence of water. It appears that water inhibits both the TH and etherification reaction. Specifically, for Hf-Beta, adding 1.45 mol of water per mol of HMF (i.e., essentially the same amount of water formed after 24 h in a typical batch reaction) resulted in a significant decrease in BEMF yield from 18% to 6% (Table 3, entries 1 and 2). When the water content was increased up to 2.4 wt%, the conversion of HMF decreased from 54% to 22% after 4 h reaction, with less than 1% BEMF yield (Table 3, entry 3). We observed a shift in selectivity towards BHMF, consistent with our results for the continuous flow reaction (Figure 2a). The results obtained for Sn-Beta suggest that this catalyst has a higher etherification activity compared to Hf-Beta. Water dissolved in ethanol can diffuse to and interact with the acid sites despite the high hydrophobicity of the defect-free pores. Water has been found to bind more strongly than methanol to Lewis acid centers in Beta zeolites, following an adsorption strength order of $Ti < Sn < Zr$.[21c] Assuming that Hf-Beta has a Lewis acid strength similar to Zr-Beta, water should have a more detrimental effect on Hf than on Sn.

Table 3. Influence of water content on the catalyst performance for the reaction of HMF with ethanol in the presence of Hf- or Sn-Beta.[a]

Entry	Catalyst	Water cont. [wt%]	Conv. [%]	Yield [%] BEMF	BHMF	EMF	HMFDEA
1	Hf-Beta	–	54	18	2	4	28
2	Hf-Beta	0.2	42	6	6	1	28
3	Hf-Beta	2.4	22	<1	13	0	6
4	Sn-Beta	–	72	33	<1	13	14
5	Sn-Beta	0.2	55	23	<1	12	15
6	Sn-Beta	2.8	11	5	<1	3	5

[a] Reactions were run for 4 h; for other reaction conditions see Table 1.

Further studies were performed by reacting HMF with 2-butanol or 1-butanol instead of ethanol (Table 4). Structural differences between the alcohols impact the polarity and hydrogen donor ability,[11e,27] and these differences are clearly manifested in the reaction kinetics and product selectivities. 2-Butanol is readily oxidized and is, therefore, an efficient hydrogen donor. The reaction of 2-butanol and HMF with Hf-Beta is the most active in the formation of the corresponding furanic diether, 2,5-bis(butoxymethyl)furan (BBMF), achieving 93% conversion in 1 h with 87% selectivity (Table 4, entry 1). Reactions with 2-butanol did not generate any acetal compounds, indicating a strong steric hindrance effect of the butyl chain. Interestingly, the catalytic activity of Hf-Beta was almost unaffected by the addition of 0.2 wt% water (Table 4, entry 2). Sn-Beta was significantly less active for the etherification of HMF with 2-butanol, converting only 43% HMF under identical conditions (Table 4, entry 7). The effect of water seems to depend on the properties of the metal because addition of 0.2 wt% water to the Sn-Beta system resulted in a larger decrease in conversion and BBMF selectivity compared with the reactions with Hf-Beta.

Significantly lower BBMF yields were obtained when using 1-butanol instead of 2-butanol as co-reactant. The most notable difference in product distribution for this primary alcohol is the presence of acetal products and 5-(butoxymethyl)furfural (BMF). Together with previous studies[9a] and calculations of re-

Table 4. Influence of the water content on the catalyst performance for the reaction of HMF with 2-butanol or 1-butanol in the presence of Hf- or Sn-Beta.[a]

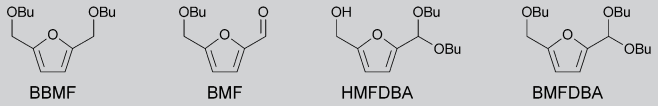

Entry	Catalyst	Solvent	Water cont. [wt%]	Conv. [%]	Yield [%] BBMF	BMF	HMFDBA/BMFDBA
1	Hf-Beta	2-butanol	–	93	81	0	0
2	Hf-Beta	2-butanol	0.2	92	79	0	0
3	Hf-Beta	2-butanol	2.1	66	<1	0	0
4	Hf-Beta	1-butanol	–	84	22	22	38
5	Hf-Beta	1-butanol	0.2	73	19	18	33
6	Hf-Beta	1-butanol	2.1	30	5	2	9
7	Sn-Beta	2-butanol	–	43	37	0	0
8	Sn-Beta	2-butanol	0.2	19	17	0	0
9	Sn-Beta	2-butanol	2.5	4	3	0	0
10	Sn-Beta	1-butanol	–	97	5	46	52
11	Sn-Beta	1-butanol	0.2	95	5	54	39
12	Sn-Beta	1-butanol	2.1	42	1	32	10

[a] Reaction conditions: 1 wt% HMF in solvent, (mol HMF)/(mol metal) = 100:3, 0.25 wt% 1,3,5-tri-*tert*-butylbenzene, 1 h, 393 K. BBMF = 2,5-bis(butoxymethyl)furan; BMF = 5-(butoxymethyl)furfural; HMFDBA = 5-(hydroxymethyl)furfural dibutyl acetal; BMFDBA = 5-(butoxymethyl)furfural dibutyl acetal; Bu = butyl.

action energetics,[14] the data support the conclusion that 2-butanol is a more effective hydrogen donor than ethanol or 1-butanol for the TH reaction.

Flow-reactor studies of the coupled TH and etherification of HMF with 2-butanol

Having demonstrated that the use of 2-butanol as a reactant increases the product selectivity towards the desired ether compound, we extended our approach to explore this reaction under continuous flow conditions (Figure 7). For the reaction with Hf-Beta, the initial BBMF selectivity was 93% at a conversion of 91%. The dependence of HMF conversion on TOS indicates that this catalyst remains active over the course of 96 h, corresponding to a TON value of 710. A striking trend observed in Figure 7a is the exponential decay in the production of BBMF. The shift in product selectivity to BHMF is again interpreted as the result of structural changes occurring at the Hf centers within the zeolite. Interestingly, calcination of the Hf-Beta catalyst at 823 K resulted in an almost complete recovery of the etherification activity, suggesting a more reversible nature of the catalyst deactivation compared to the reaction performed in ethanol.

A very different behavior was found for Sn-Beta (Figure 7b), which was tested at a significantly lower WHSV compared to Hf-Beta (3.8 vs. 58.1 h^{-1}) owing to its lower TH activity. Initially, the catalytic activity decreased from 75 to 57% HMF conversion after 5 h; however, the catalyst appeared to be very stable over the next 100 h. Specifically, Sn-Beta showed a remarkably high selectivity for the etherification of HMF with 2-butanol, yielding 40% BBMF at 51% conversion and a TON of 120 after 105 h on stream. No significant formation of BHMF or 5-(butoxymethyl)furfuryl alcohol (BMFA) was observed at this stage. When compared at an identical TON, Hf-Beta yielded only 25% BBMF at 78% conversion. The different behavior of Hf- and Sn-Beta in ethanol and 2-butanol seems to suggest a strong sensitivity to the polarity of the medium for the coupled TH and etherification of HMF.

Conclusions

We have demonstrated that the zeolites Hf-, Zr-, and Sn-Beta promote the coupled transfer hydrogenation and etherification reaction of HMF with primary and secondary alcohols. The reactivity of these Lewis acid catalysts has been investigated in a continuous flow reactor, and the results were related to extensive characterization studies of the catalytic sites. Sn-Beta showed the highest stability and selectivity for etherification whereas Hf- and Zr-Beta appeared to be more active in the Meerwein–Ponndorf–Verley (MPV) reduction. We are especially intrigued by the selec-

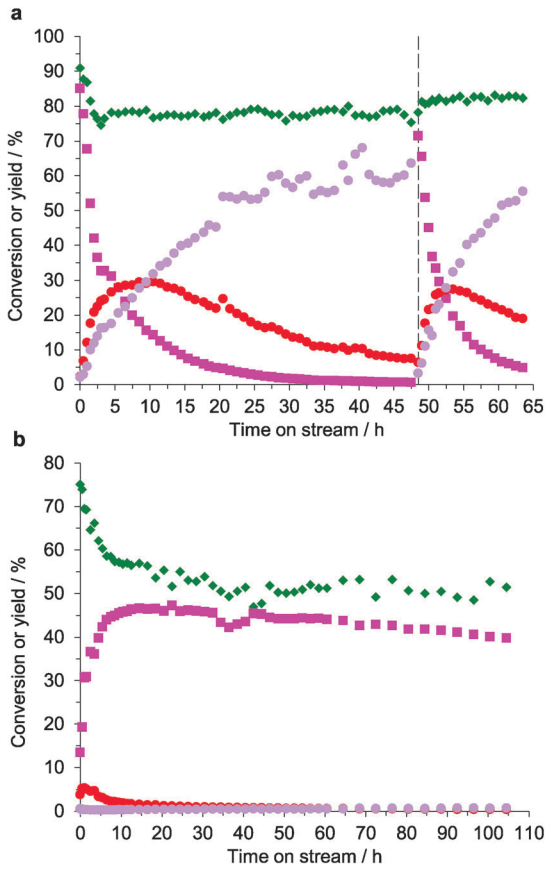

Figure 7. HMF conversion (◆) and yields of BBMF (■), BMFA (●), and BHMF (●) as a function of TOS for flow reactions with a) Hf-Beta and b) Sn-Beta. Reaction conditions: 1 wt% HMF in 2-butanol, 0.25 wt% 1,3,5-tri-*tert*-butylbenzene, 393 K, 100 psig. The operating conditions of the flow reactor were: For Hf-Beta, 301 mg catalyst (Si/Hf ratio of 92), WHSV of 58.1 h^{-1}, flow rate of 0.4 mL min^{-1}; and for Sn-Beta, 597 mg catalyst (Si/Sn ratio of 119), WHSV of 3.8 h^{-1}, flow rate of 0.05 mL min^{-1}. Regeneration of Hf-Beta was performed by calcination in air at 823 K for 5 h (indicated by the dashed line).

tive product distribution and superior catalyst stability in the Sn-Beta-catalyzed reaction of HMF with 2-butanol. Research into combining such Lewis acid zeolites with a heterogeneous Brønsted acid in a dual catalyst bed system is needed to ultimately advance a breakthrough in the continuous and scalable production of HMF ethers.

Taken together, our results provide new insights into the changes of the local environment near the metal centers within the zeolites and show, for the first time, the partially reversible deactivation of these materials in a flow reactor. Efforts to expand the scope of continuous flow strategies to other types of Lewis acid-catalyzed cascade reactions are currently underway in our group.

Experimental Section

Catalyst synthesis

The zeolites were synthesized based on the procedure reported by Corma et al.[20c] using the following precursors: hafnium(IV) chloride, zirconium(IV) oxychloride octahydrate, tin(II) chloride dihydrate, titanium(IV) isopropoxide, tantalum(V) ethoxide, and niobium(V) ethoxide. Tin(II), which oxidizes to tin(IV) in water, was used in place of $SnCl_4{\cdot}5H_2O$ and resulted in Sn-Beta consistently free of extra-framework SnO_2.[28] Hf-Beta was synthesized as follows: aqueous tetraethylammonium hydroxide [27.158 g; Sigma–Aldrich, 35 wt% (TEAOH)] and tetraethylorthosilicate (23.968 g; Sigma–Aldrich, 99 wt%) were added to a Teflon [polytetrafluoroethylene (PTFE)] dish, which was magnetically stirred at room temperature for 90 min. Additional deionized water (15 mL) was added, and the dish was cooled in an ice bath. Then, hafnium(IV) chloride (0.3747 g; Sigma–Aldrich, 98 wt%) dissolved in ethanol (2 mL) was added dropwise. The solution was left uncovered on a stir plate for 10 h to reach a total mass of 33.147 g after evaporation of ethanol and some of the water. Next, aqueous hydrofluoric acid (2.620 g; Sigma–Aldrich, 48 wt%) was added dropwise, and the mixture was homogenized using a PTFE spatula, resulting in a thick gel. Si-Beta (0.364 g), prepared using an identical procedure without seeding or hafnium(IV) chloride addition, was seeded into the mixture. The weight of the resulting sol–gel was allowed to be reduced to 33.956 g over roughly 2 h, which corresponds to a final molar composition of $1\ SiO_2/0.01\ HfCl_4/0.56$ TEAOH/0.56 HF/$7.5\ H_2O$. The thick paste was transferred to a PTFE-lined stainless steel autoclave (45 mL) and heated to 413 K for 20 days under static conditions. The solids were recovered by filtration, washed with nanopure H_2O, and dried at 373 K. The zeolites were calcined by heating to 853 K with a $1\ K\,min^{-1}$ ramp (with 1 h isothermal steps at 423 and 623 K) and kept at that temperature for 10 h. After calcination, the overall inorganic oxide yield was 80–90%. HfO_2/Si-Beta was prepared by incipient wetness impregnation of Si-Beta with an aqueous hafnium(IV) chloride solution, followed by drying at 383 K and calcination in air flow at 533 K. Sn- and Zr-MCM-41 were synthesized according to previously published protocols.[29] All catalysts were synthesized to achieve a silicon/metal ratio of roughly 100 (see Table 1).

Catalytic reactions

Batch reactions were carried out in a glass reactor (5 mL) under autogenous pressure and heated in a temperature-controlled oil bath with magnetic stirring. The temperature in the reaction vial was measured by a K-type thermocouple (Omega) placed inside the liquid mixture and controlled to 393 K. The reactors were charged with the reactant solution (2.5 mL, 1 wt% HMF in alcoholic solvent), an internal standard (1,3,5-tri-*tert*-butylbenzene), and the desired amount of catalyst (corresponding to a ratio of mol metal/mol HMF of 3:100). The reactions were allowed to proceed for the times designated within Tables 1, 3, and 4 and Figure 1. Afterwards, the sample was prepared for analysis by passing the liquid through a 0.2 μm Millipore PTFE syringe filter to remove extraneous particulates. Flow reactions were conducted in a $^1/_4$ inch tubular stainless steel reactor mounted inside an aluminum block within an insulated single-zone furnace (850 W/115 V, Applied Test Systems Series 3210). The catalyst bed consisted of the calcined catalyst loaded between quartz wool plugs and supported by inert glass beads. The reaction temperature was monitored inside the reactor using a K-type thermocouple (Omega). The system was pressurized with dry compressed air. This pressure was controlled by a backpressure regulator. Liquid reactants were introduced into the reactor by using a Waters 515 HPLC pump, and the effluent was collected in a separator (Gage & Valve Co.) at room temperature. Each experiment was carried out at 393 K and 791 kPa. The effluent liquid was drained periodically for analysis.

Product analysis

Liquid samples were analyzed using an Agilent Technologies 6890N GC equipped with an Agilent DB-1701 capillary column (length 30 m; inner diameter 0.25 mm; film thickness 0.25 μm) and flame ionization detector (split ratio 20:1, column flow rate $2.4\ mL\ min^{-1}$). Product identification was performed by GC–MS using an Agilent 7890A GC equipped with a DB-1701 capillary column (30 m × 0.25 mm) and compared with available standard compounds. HMF ether and acetal compounds were synthesized and purified according to the methods described by Balakrishnan et al.[5c]

Catalyst characterization

ICP-AES were recorded on an Optima 2000 DV spectrometer (PerkinElmer Inc.). PXRD patterns were collected using a Bruker D8 diffractometer using CuK_α radiation. UV/Vis analysis was performed using a Varian Cary 5000 UV/Vis NIR spectrometer equipped with a Praying Mantis diffuse reflectance accessory. The spectra were collected at 190–450 nm and referenced to $BaSO_4$. TGA was performed by heating the catalyst under a flow of $10\ mL\,min^{-1}\ N_2$ and $90\ mL\,min^{-1}$ air using a Q500 thermal analysis system (TA Instruments). After 1 h dehydration at 423 K, approximately 30 mg of the sample was heated to 1073 K ($5\ K\,min^{-1}$). FTIR spectra were acquired using a Bruker Vertex 70 spectrophotometer. Approximately 10 mg samples were pressed into 13 mm self-supporting pellets and placed into a Harrick high temperature FTIR cell. Each sample was heated to 623 K ($10\ K\,min^{-1}$) and held for 1 h under flowing He. Once the cell had cooled to room temperature, dynamic vacuum of a pressure of roughly 0.1 Pa was established. A reference spectrum was then acquired. Under a static vacuum, the cell was dosed with excess CD_3CN vapor. The vapor was evacuated after 10 min, and the cell was dosed once more. Once dynamic vacuum was re-established, the difference spectrum was acquired. N_2 adsorption–desorption isotherms were measured on a Quantachrome Autosorb iQ apparatus at the liquid-nitrogen temperature (77 K). All samples were degassed under vacuum prior to use (623 K, 12 h). Micropore volumes were analyzed by the t-plot method.

^{13}C, ^{119}Sn, and ^{29}Si MAS NMR experiments

MAS NMR experiments were performed on custom-designed spectrometers (courtesy of D. J. Ruben, Francis Bitter Magnet Laboratory, Massachusetts Institute of Technology) operating at 360, 400, and 500 MHz (^1H Larmor frequency). The 360 MHz (8.4 T) spectrometer was equipped with either a double resonance homebuilt (FBML-MIT) or a triple resonance Varian-Chemagnetics probe (Palo Alto, CA), which were doubly tuned to $^{119}Sn/^1H$. The 400 MHz (9.4 T) spectrometer was equipped with a homebuilt (FBML-MIT) double resonance probe doubly tuned to $^{29}Si/^1H$. The 500 MHz (11.7 T) spectrometer was equipped with a triple resonance Varian-Chemagnetics probe (Palo Alto, CA) doubly tuned to $^{13}C/^1H$. Powdered samples were packed into either 3.2 mm (26 and 36 μL fill volume) or 4 mm (80 μL fill volume) outer diameter ZrO_2 rotors equipped with Vespel drive- and top-caps. Top-caps were equipped with rubber O-ring seals to inhibit water contamination of the sample (Revolution NMR, Fort Collins, CO). Dry samples were prepared by heating to 473 K under a 10 Pa vacuum and packing the NMR rotor in an Ar-filled glovebox. Sample temperatures were maintained between 294 and 300 K. ^{119}Sn MAS NMR spectra were acquired by performing a Hahn-echo (^{119}Sn, $\omega_1/2\pi =$ 50 kHz) and cross-polarization (CP) experiments with recycle delays between 4 and 30 s, between 10 240 and 35 850 scans, and a spinning frequency of $\omega_r/2\pi = 8$ kHz. CP experiments were acquired with contact times between 0.4 and 4 ms. ^{119}Sn spectra were referenced using powdered SnO_2 (−604.3 ppm) as an external standard relative to trimethyltin (0 ppm). $^{13}C\{^1H\}$ CP MAS NMR spectra were acquired using a 4 s recycle delay, $\omega_r/2\pi = 8$ kHz, 51 200 scans, a contact time of 1.5 ms, and high-power ^1H decoupling (TPPM, $\omega_1/2\pi = 83$ kHz). ^{13}C NMR spectra were referenced with respect to adamantane [38.48 ppm, relative to tetramethylsilane (TMS)]. ^{29}Si NMR spectra were acquired using a Hahn-echo (^{29}Si, $\omega_1/2\pi =$ 50 kHz), recycle delay between 30 and 120 s, $\omega_r/2\pi = 10$ kHz, and between 3 584 and 4 096 scans. ^{29}Si data were referenced to 0 ppm using TMS.

List of Abbreviations

BBMF	2,5-Bis(butoxymethyl)furan
BEMF	2,5-Bis(ethoxymethyl)furan
BHMF	2,5-Bis(hydroxymethyl)furan
BMF	5-(Butoxymethyl)furfural
BMFA	5-(Butoxymethyl)furfuryl alcohol
BMFDBA	5-(Butoxymethyl)furfural dibutyl acetal
CD_3CN	Deuterated acetonitrile
CP	Cross-polarization
EL	Ethyl levulinate
EMF	5-(Ethoxymethyl)furfural
EMFA	5-(Ethoxymethyl)furfuryl alcohol
EMFDEA	5-(Ethoxymethyl)furfural diethyl acetal
EtOH	Ethanol
FID	Flame ionization detector
FTIR	Fourier transform infrared spectroscopy
HMF	5-(Hydroxymethyl)furfural
HMFDBA	5-(Hydroxymethyl)furfural dibutyl acetal
HMFDEA	5-(Hydroxymethyl)furfural diethyl acetal
ICP-AES	Inductively coupled plasma atomic emission spectrometry
MAS NMR	Magic-angle spinning nuclear magnetic resonance
MeCHO	Acetaldehyde
MPV	Meerwein–Ponndorf–Verley
PTFE	Polytetrafluoroethylene
PXRD	Powder X-ray diffraction
RT	Room temperature
TEAOH	Tetraethylammonium hydroxide
TGA	Thermogravimetric analysis
TH	Transfer hydrogenation
TMS	Tetramethylsilane
TON	Turnover number
TOS	Time on stream
UV/Vis	Ultraviolet/visible light
WHSV	Weight hourly space velocity

Acknowledgements

This work was sponsored by the Chemical Sciences, Geosciences and Biosciences Division, Office of Basic Energy Sciences, Office of Science, U.S. Department of Energy, under Award No. DE-FG0212ER16352. J.D.L. was partially supported by the National Science Foundation Graduate Research Fellowship under Grant No. 122374. Any opinion, findings, and conclusions or recommendations expressed in this material are those of the authors(s) and do not necessarily reflect the views of the National Science Foundation. S.V.d.V. was partially supported by the Research Foundation—Flanders (FWO). NMR studies were supported through the National Institutes of Health (NIH grants EB001960 and EB002026). V.K.M. was partially funded by the Natural Sciences and Engineering Research Council of Canada Postdoctoral Fellowship Program. We thank S. Hunt and Y. Wang for ICP-AES analyses, H. Luo for N_2 adsorption experiments and assistance with the UV/Vis measurements, and F. Leibfarth for the purification of the HMF ether and acetal compounds.

Keywords: biomass conversion · cascade reactions · hydrogen transfer · solid lewis acids · zeolites

[1] a) T. Wang, M. W. Nolte, B. H. Shanks, *Green Chem.* **2014**, *16*, 548–572; b) S. Van de Vyver, Y. Román-Leshkov, *Catal. Sci. Technol.* **2013**, *3*, 1465–1479; c) J.-P. Lange, E. van der Heide, J. van Buijtenen, R. Price, *ChemSusChem* **2012**, *5*, 150–166; d) C. Aellig, I. Hermans, *ChemSusChem* **2012**, *5*, 1737–1742; e) S. Dutta, S. De, B. Saha, *ChemPlusChem* **2012**, *77*, 259–272; f) S. Van de Vyver, J. Geboers, P. A. Jacobs, B. F. Sels, *ChemCatChem* **2011**, *3*, 82–94; g) J. C. Serrano-Ruiz, J. A. Dumesic, *Energy Environ. Sci.* **2011**, *4*, 83–99; h) E. Taarning, C. M. Osmundsen, X. Yang, B. Voss, S. I. Andersen, C. H. Christensen, *Energy Environ. Sci.* **2011**, *4*, 793–804; i) D. M. Alonso, J. Q. Bond, J. A. Dumesic, *Green Chem.* **2010**, *12*, 1493–1513; j) J. N. Chheda, G. W. Huber, J. A. Dumesic, *Angew. Chem. Int. Ed.* **2007**, *46*, 7164–7183; *Angew. Chem.* **2007**, *119*, 7298–7318; k) J. O. Metzger, *Angew. Chem. Int. Ed.* **2006**, *45*, 696–698; *Angew. Chem.* **2006**, *118*, 710–713.

[2] a) G. W. Huber, J. N. Chheda, C. J. Barrett, J. A. Dumesic, *Science* **2005**, *308*, 1446–1450; b) R. M. West, Z. Y. Liu, M. Peter, J. A. Dumesic, *ChemSusChem* **2008**, *1*, 417–424; c) R. M. West, Z. Y. Liu, M. Peter, C. A. Gärtner, J. A. Dumesic, *J. Mol. Catal. A* **2008**, *296*, 18–27; d) A. D. Sutton, F. D. Waldie, R. L. Wu, M. Schlaf, L. A. Silks, J. C. Gordon, *Nat. Chem.* **2013**, *5*, 428–432; e) W. Shen, G. A. Tompsett, K. D. Hammond, R. Xing, F. Dogan, C. P. Grey, W. C. Conner, Jr., S. M. Auerbach, G. W. Huber, *Appl. Catal. A* **2011**, *392*, 57–68.

[3] a) Y. Román-Leshkov, C. J. Barrett, Z. Y. Liu, J. A. Dumesic, *Nature* **2007**, *447*, 982 – 985; b) S. De, S. Dutta, B. Saha, *ChemSusChem* **2012**, *5*, 1826 – 1833; c) X. Tong, Y. Ma, Y. Li, *Appl. Catal. A* **2010**, *385*, 1 – 13; d) M. Chidambaram, A. T. Bell, *Green Chem.* **2010**, *12*, 1253 – 1262; e) K. L. Deutsch, B. H. Shanks, *J. Catal.* **2012**, *285*, 235 – 241; f) A. Takagaki, M. Takahashi, S. Nishimura, K. Ebitani, *ACS Catal.* **2011**, *1*, 1562 – 1565.

[4] a) M. M. Antunes, P. A. Russo, P. V. Wiper, J. M. Veiga, M. Pillinger, L. Mafra, D. V. Evtuguin, N. Pinna, A. A. Valente, *ChemSusChem* **2014**, *7*, 804 – 812; b) J. Chen, G. Zhao, L. Chen, *RSC Adv.* **2014**, *4*, 4194 – 4202.

[5] a) E. Salminen, N. Kumar, P. Virtanen, M. Tenho, P. Mäki-Arvela, J.-P. Mikkola, *Top. Catal.* **2013**, *56*, 765 – 769; b) H. Wang, T. Deng, Y. Wang, Y. Qi, X. Hou, Y. Zhu, *Bioresour. Technol.* **2013**, *136*, 394 – 400; c) G. A. Kraus, T. Guney, *Green Chem.* **2012**, *14*, 1593 – 1596; d) C. M. Lew, N. Rajabbeigi, M. Tsapatsis, *Ind. Eng. Chem. Res.* **2012**, *51*, 5364 – 5366; e) M. Balakrishnan, E. R. Sacia, A. T. Bell, *Green Chem.* **2012**, *14*, 1626 – 1634; f) P. Lanzafame, D. M. Temi, S. Perathoner, G. Centi, A. Macario, A. Aloise, G. Giordano, *Catal. Today* **2011**, *175*, 435 – 441; g) M. Mascal, E. B. Nikitin, *ChemSusChem* **2009**, *2*, 423 – 426; h) M. Mascal, E. B. Nikitin, *ChemSusChem* **2009**, *2*, 859 – 861; i) M. Mascal, E. B. Nikitin, *Angew. Chem. Int. Ed.* **2008**, *47*, 7924 – 7926; *Angew. Chem.* **2008**, *120*, 8042 – 8044.

[6] E. de Jong, T. Vijlbrief, R. Hijkoop, G.-J. M. Gruter, J. C. van der Waal, *Biomass Bioenergy* **2012**, *36*, 151 – 159.

[7] G. J. M. Gruter, US8277521 B2, **2012**.

[8] G. J. M. Gruter, US8231693 B2, **2012**.

[9] a) J. Jae, E. Mahmoud, R. F. Lobo, D. G. Vlachos, *ChemCatChem* **2014**, *6*, 508 – 513; b) A. Corma, F. X. Llabrés i Xamena, C. Prestipino, M. Renz, S. Valencia, *J. Phys. Chem. C* **2009**, *113*, 11306 – 11315; c) A. Corma, M. Renz, *Angew. Chem. Int. Ed.* **2007**, *46*, 298 – 300; *Angew. Chem.* **2007**, *119*, 302 – 304.

[10] a) M. Chia, J. A. Dumesic, *Chem. Commun.* **2011**, *47*, 12233 – 12235; b) D. Scholz, C. Aellig, I. Hermans, *ChemSusChem* **2014**, *7*, 268 – 275; c) X. Wang, R. Rinaldi, *Energy Environ. Sci.* **2012**, *5*, 8244 – 8260.

[11] a) M. Moliner, *Dalton Trans.* **2014**, *43*, 4197 – 4208; b) Y. Román-Leshkov, M. E. Davis, *ACS Catal.* **2011**, *1*, 1566 – 1580; c) W. R. Gunther, Y. R. Wang, Y. W. Ji, V. K. Michaelis, S. T. Hunt, R. G. Griffin, Y. Román-Leshkov, *Nat. Commun.* **2012**, *3*, 1109 – ; d) A. Corma, M. E. Domine, L. Nemeth, S. Valencia, *J. Am. Chem. Soc.* **2002**, *124*, 3194 – 3195; e) A. Corma, M. E. Domine, S. Valencia, *J. Catal.* **2003**, *215*, 294 – 304; f) M. Boronat, A. Corma, M. Renz, *J. Phys. Chem. B* **2006**, *110*, 21168 – 21174.

[12] L. Bui, H. Luo, W. R. Gunther, Y. Román-Leshkov, *Angew. Chem. Int. Ed.* **2013**, *52*, 8022 – 8025; *Angew. Chem.* **2013**, *125*, 8180 – 8183.

[13] M. J. Climent, A. Corma, S. Iborra, M. J. Sabater, *ACS Catal.* **2014**, *4*, 870 – 891.

[14] R. S. Assary, L. A. Curtiss, J. A. Dumesic, *ACS Catal.* **2013**, *3*, 2694 – 2704.

[15] J. C. van der Waal, E. J. Creyghton, P. J. Kunkeler, K. Tan, H. van Bekkum, *Top. Catal.* **1997**, *4*, 261 – 268.

[16] P. G. M. Wuts, T. W. Greene in *Greene's Protective Groups in Organic Synthesis*, Wiley, **2006**, pp. 431 – 532.

[17] Y. Zhu, G.-K. Chuah, S. Jaenicke, *J. Catal.* **2006**, *241*, 25 – 33.

[18] a) I. van Zandvoort, Y. Wang, C. B. Rasrendra, E. R. H. van Eck, P. C. A. Bruijnincx, H. J. Heeres, B. M. Weckhuysen, *ChemSusChem* **2013**, *6*, 1745 – 1758; b) S. Van de Vyver, J. Thomas, J. Geboers, S. Keyzer, M. Smet, W. Dehaen, P. A. Jacobs, B. F. Sels, *Energy Environ. Sci.* **2011**, *4*, 3601 – 3610.

[19] M. H. Tucker, A. J. Crisci, B. N. Wigington, N. Phadke, R. Alamillo, J. Zhang, S. L. Scott, J. A. Dumesic, *ACS Catal.* **2012**, *2*, 1865 – 1876.

[20] a) R. Bermejo-Deval, R. S. Assary, E. Nikolla, M. Moliner, Y. Román-Leshkov, S.-J. Hwang, A. Palsdottir, D. Silverman, R. F. Lobo, L. A. Curtiss, M. E. Davis, *Proc. Natl. Acad. Sci. USA* **2012**, 9727 – 9732; b) R. Bermejo-Deval, R. Gounder, M. E. Davis, *ACS Catal.* **2012**, *2*, 2705 – 2713; c) A. Corma, L. T. Nemeth, M. Renz, S. Valencia, *Nature* **2001**, *412*, 423 – 425.

[21] a) S. Roy, K. Bakhmutsky, E. Mahmoud, R. F. Lobo, R. J. Gorte, *ACS Catal.* **2013**, *3*, 573 – 580; b) C. M. Osmundsen, M. S. Holm, S. Dahl, E. Taarning, *Proc. R. Soc. A* **2012**, *468*, 2000 – 2016; c) B. S. Kulkarni, S. Krishnamurty, S. Pal, *J. Mol. Catal. A* **2010**, *329*, 36 – 43; d) M. Boronat, P. Concepción, A. Corma, M. Renz, *Catal. Today* **2007**, *121*, 39 – 44; e) M. Boronat, P. Concepción, A. Corma, M. Renz, S. Valencia, *J. Catal.* **2005**, *234*, 111 – 118.

[22] J. Chen, J. M. Thomas, G. Sankar, *J. Chem. Soc. Faraday Trans.* **1994**, *90*, 3455 – 3459.

[23] a) K. S. Arias, M. J. Climent, A. Corma, S. Iborra, *ChemSusChem* **2014**, *7*, 210 – 220; b) R. H. Clark, W. E. Graham, A. G. Winter, *J. Am. Chem. Soc.* **1925**, *47*, 2748 – 2754.

[24] X. X. Wang, F. Lefebvre, J. Patarin, J.-M. Basset, *Microporous Mesoporous Mater.* **2001**, *42*, 269 – 276.

[25] F. de Clippel, M. Dusselier, R. van Rompaey, P. Vanelderen, J. Dijkmans, E. Makshina, L. Giebeler, S. Oswald, G. V. Baron, J. F. M. Denayer, P. P. Pescarmona, P. A. Jacobs, B. F. Sels, *J. Am. Chem. Soc.* **2012**, *134*, 10089 – 10101.

[26] J.-P. Gallas, J.-M. Goupil, A. Vimont, J.-C. Lavalley, B. Gil, J.-P. Gilson, O. Miserque, *Langmuir* **2009**, *25*, 5825 – 5834.

[27] C. Reichardt, T. Welton in *Solvents and Solvent Effects in Organic Chemistry*, Wiley-VCH, Weinheim, **2010**, pp. 425 – 508.

[28] W. R. Gunther, Q. Duong, Y. Román-Leshkov, *J. Mol. Catal. A* **2013**, *379*, 294 – 302.

[29] a) H. Y. Luo, L. Bui, W. R. Gunther, E. Min, Y. Román-Leshkov, *ACS Catal.* **2012**, *2*, 2695 – 2699; b) T. R. Gaydhankar, P. N. Joshi, P. Kalita, R. Kumar, *J. Mol. Catal. A* **2007**, *265*, 306 – 315.

Received: February 24, 2014
Revised: March 30, 2014
Published online on July 8, 2014